CONCURRENT MEASUREMENT OF SPINDLE RADIAL, AXIAL AND ANGULAR MOTIONS USING CONCENTRIC CIRCLE GRATING AND PHASE MODULATION INTERFEROMETERS

Masato AKETAGAWA[1], Mumummad MADDEN[1] and Eiki OKUYAMA[2]

1 Nagaoka University of Technology, Nagaoka, Niigata 940-2188, Japan, masatoaa@vos.nagaokaut.ac.jp
*2 Akita University, Akita 010-8502, Jap*an

Abstract:

This paper describes a concurrent measurement of spindle radial, axial and angular motions using concentric circle grating and phase modulation interferometers. In the measurement, the concentric circle grating with fine pitch is a reference artifact. A frequency modulated laser diode is used for the light source of the phase modulation interferometers. The phase modulation interferometers, which consist of three Michelson and three grating interferometers, measure three radial and three axial displacements of the grating. From these six measured displacements, radial, axial and angular motions of the spindle can be determined concurrently. In the paper, a measurement principle, a measurement instrument and experimental results are discussed. Concurrent measurements of spindle radial, axial and angular motions were successfully attained.

Keywords: spindle, radial motion, axial motion, angular motion, concentric circle grating, phase modulation

1. INTRODUCTION

The industrial processes for ultra-precision engineering and metrology require the fine quality control of products. The precision of rotary spindle is also required to enhance the accuracy of spindle motions to the nanometer and sub-µradian levels [1, 2]. The ideal spindles must have only rotary motion with one degree of freedom, therefore, another extra motions with five degrees of freedom (= radial (2 degrees) + axial (1 degree) + angular (2 degrees)) are identified as error motions, which must be eliminated or reduced. Conventional spindle error motion measurements are the error separation methods [3-5], which require artifact reference and displacement sensors, such as capacitive sensors. Radial error motion can be measured using a precise sphere or circular cylinder as the reference artifact [3-5]. A concentric circle grating is also used as the reference artifact for measuring the radial error motion [6, 7]. A precise circular cylinder with end mirror surface can be used as the reference artifact for the concurrent measurement of (radial + axial) or (axial + angular) motions [8, 9]. Using a sphere ball as the reference artifact, the spindle error motions (radial (2 degrees) + axial (1 degree)) can be measured [10]. In addition, the concurrent measurement of radial (2 degrees), axial (1 degree) and angular (2 degrees) motions can be realized using the reference artifact of two sphere balls linked with a cylinder [10]. However, in the concurrent measurement of radial, axial and angular motions, this artifact is voluminous and has too much mass to have the possibility of inhibiting the original rotational motion of the spindle. Moreover, capacitive sensors have narrow bandwidths, and maintaining the traceability against the meter definition is difficult because of their drift characteristic. As similar examples for multi-axes displacement measurement, 2-dimensional grating mirrors are used as fixed and moving mirrors in Michelson interferometers [11, 12].

This paper describes a concurrent measurement of spindle radial, axial and angular motions using a concentric circle grating and phase modulation interferometers. In this method, the concentric circle grating plate with a fine pitch is installed on top of the spindle of interest and is used as the reference artifact. Because the concentric circle grating plate is not voluminous and not heavy, this method is effective for any spindle, and does not affect the spindle original rotational motion. Since this method is based on wide-bandwidth photo sensors, it is possible to apply it to high-rotational-speed spindles. Moreover, this method is suitable for maintaining the traceability against the meter definition, if the grating pitch and the wavelength are calibrated.

2. PRINCIPLE

Figure 1 shows the measurement system of the spindle error motions using the three optical sensors and the concentric circle grating. In the system, the Z-axis is the ideal rotation axis for the spindle. A concentric circle grating is set on top of the spindle of interest. Three optical sensors A, B and C are fixed over the concentric circle grating. The spindle rotation center must be nearly aligned to the center of the concentric circle grating. The grating plane must be aligned to be nearly parallel with the XY plane with in 10 arcsecond. In figure 1, the spindle rotation center is selected as the origin point of the XYZ coordinate system. The optical sensor A is located along the Y-axis with the distance R_A from the center and measures the Y-axis and Z-axis displacements y_A and z_A, whereas the optical sensor B and C are located along the X-axis with the distances R_B and R_C from the center, and measure the X-axis and Z-axis displacements x_B, z_B, x_C and z_C. From the measured displacements by the three optical sensors, the radial R_x, R_y, axial R_z and angular θ_x, θ_y motions can be derived as [13]
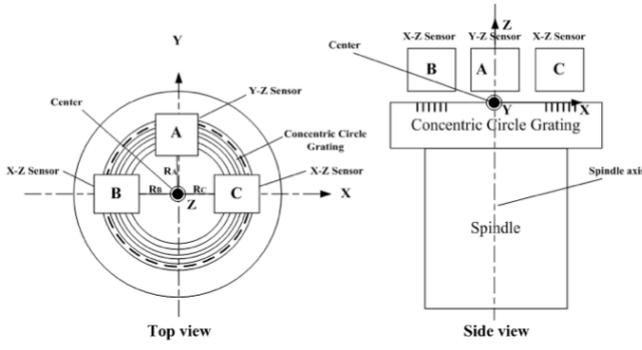
Figure 1 Basic principle of spindle error motion measurement

$$R_x = \frac{1}{2}(x_B + x_C) \tag{1},$$

$$R_y = y_A \tag{2},$$

$$R_Z = \frac{1}{3}(z_A + z_B + z_C) \tag{3},$$

$$\theta_x = \frac{1}{R}\left\{z_A - \frac{(z_A + z_C)}{2}\right\} \tag{4},$$

$$\theta_y = \frac{1}{2R}(z_B - z_C) \tag{5},$$

$$R = \frac{1}{3}(R_A + R_B + R_C) \tag{6},$$

where R is the averaged distance of the interferometers A, B and C from the center.
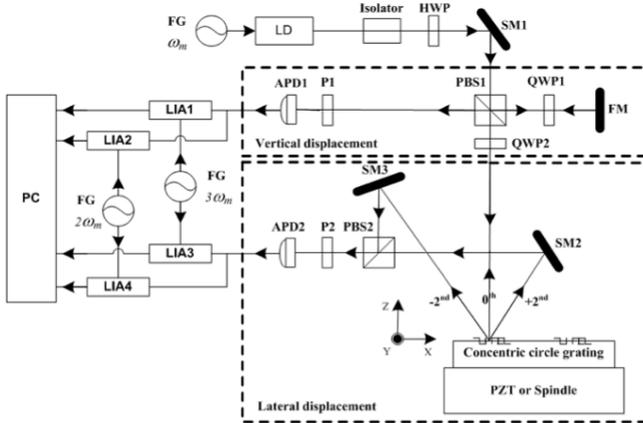

Figure 2 Schematic diagram of the optical sensor. LD: laser diode; SM: steering mirror; FM: fixed mirror; HWP: half-wave plate; QWP: quarter-wave plate; PBS: polarized beam splitter; P: polarizer; APD: avalanche photodetector; LIA: lock-in amplifier, FG: function generator, PC: personal computer.

The optical sensor consists of a frequency modulated laser diode (LD) as a light source, and two interferometers. The configuration of the optical sensor is shown in **figure 2**. To obtain displacements (Lissajous diagram), we apply the sinusoidal phase modulation techniques [14, 15] to the light source of LD. We use the frequency modulation of LD. The sinusoidal angular modulation frequency is ω_m. One interferometer observes an interference fringe between reflected light from a fixed mirror (FM) and 0-th order

diffraction light from the grating. In this case, a light beam emitted from the laser is incident on polarized beam splitter 1 (PBS1), and then, it is divided into two beams. The first beam reflected from PBS1 enters the fixed mirror (FM) via quarter-wave plate 1 (QWP1) and bounces from FM and reaches avalanche photo detector 1 (APD1) via PBS1 and polarizer 1 (P1). The second beam, which goes through PBS1, reaches the concentric circle grating via QWP2. In figure 2, we assume that the incident angle θ_i of the second beam to the grating is almost null. Thus, the reflected light (= 0-th order diffraction light) reaches APD1 via QWP2, PBS1 and P1. At APD1, it is possible to detect an interferometer fringe between the reflection lights from FM and the grating, and to measure the displacement along the Z-axis of the grating. Another interferometer observes an interference fringe between +2nd and -2nd order diffraction lights from the concentric circle grating. We use +2nd and -2nd order diffraction lights, because the lights are stronger than the other order diffraction lights. In this case, the +2nd and -2nd order diffraction lights from the grating through the steering mirror 2/3 (SM2/3) and reaches avalanche photo detector 2 (APD2) via PBS2 and polarizer 2 (P2). The observed light intensity of I_{0F} and $I_{\pm2}$ at APD1 and APD2 is represented as

$$I_{0F} = |E_0|^2 + |E_F|^2 + 2E_0 E_F \cos\left\{\varphi_{int0} - \frac{4\pi n}{c} f(L_{int0} + \Delta z)\right\} \tag{7},$$

$$I_{\pm2} = |E_{+2}|^2 + |E_{-2}|^2 + 2E_{+2} E_{-2} \cos\left\{\varphi_{int\pm2} - \frac{4\pi n}{c} f L_{int\pm2} - \frac{8\pi}{d}\Delta x\right\} \tag{8},$$

where E_0, E_F, E_{+2}, E_{-2}, φ_{int0}, $\varphi_{int\pm2}$, n, c, f, d, L_{int0}, $L_{int\pm2}$, Δx and Δz are the amplitudes of the lights reflected from 0th order diffraction of the grating and FM, the amplitudes of the lights diffracted from $\pm$2nd order of the grating, the initial phase of the 0th order interferometer, the initial phase of the $\pm$2nd order interferometer, the refractive index of air, the speed of light, the frequency of the light source, the grating pitch, the optical path difference of the 0th order interferometer arms, the optical path difference of the $\pm$2nd order interferometer arms, lateral and vertical displacements of the grating respectively. We add small modulation to the frequency of LD as

$$f = f_0 + \Delta f \tag{9},$$

where f_0 and Δf are the center frequency and modulation. We assume that Δf is negligibly smaller than f_0 (i.e. the wavelength modulation $\Delta\lambda$ is negligibly smaller than the wavelength λ). Then, in the equation (7), the second content of the blanket can be calculated as

$$\begin{aligned}&\frac{4\pi n}{c}(f_0 + \Delta f)(L_{int0} + \Delta z)\\&= \frac{4\pi n}{c}f_0(L_{int0} + \Delta z) + \frac{4\pi n}{c}\Delta f L_{int0} - \frac{4\pi n}{\lambda^2}\Delta z \Delta\lambda\end{aligned} \tag{10}.$$

In the system, the vertical displacement Δz is assumed to be the same order of the wavelength of the LD (i.e. $\Delta z \sim \lambda$), then the last term of the equation (10) can be eliminated.

Therefore, the equation (7) can be represented as,

$$I_{0F} = |E_0|^2 + |E_F|^2 + 2E_0E_F \cos\left\{\varphi'_{int0} - \frac{4\pi n}{c}f_0\Delta z - \frac{4\pi n}{c}\Delta f L_{int0})\right\} \quad (11),$$

$$\varphi'_{int0} = \varphi_{int0} - \frac{4\pi n}{c}f_0 L_{int0} \quad (12),$$

where φ'_{int0} is also an initial phase of the interferometer. We add the sinusoidal modulation to ($-\frac{4\pi n}{c}\Delta f L_{int0}$) using

$$-\frac{4\pi n}{c}\Delta f L_{int0} = k_{m0}\sin\omega_m t \quad (13),$$

where k_{m0} is the modulation index. By combining of the equations (11) and (13) and using the Bessel function ($J_m(k)$, k: modulation index, m=1, 2, 3, …), we can obtain,

$$I_{0F} = |E_0|^2 + |E_F|^2$$
$$+2E_0E_F\left[\begin{array}{l}\cos(\varphi'_{int} - \frac{4\pi n}{c}f_0\Delta z)\left\{J_0(k_{m0}) + 2\sum_{m=1}^{\infty}J_{2m}(k_{m0})\cos 2m\omega_m t\right\}\\-\sin(\varphi'_{int} - \frac{4\pi n}{c}f_0\Delta z)\left\{2\sum_{m=1}^{\infty}J_{2m+1}(k_{m0})\cos(2m+1)\omega_m t\right\}\end{array}\right] \quad (14).$$

In order to reduce the effect from the amplitude modulation of LD, we select 2nd-harmonic ($2\omega_m$) and 3rd-harmonic ($3\omega_m$). We apply the reference signal of 2nd-harmonic cosine wave ($\cos 2\omega_m t$) and the reference signal of 3rd harmonic sine wave ($\sin 3\omega_m t$) to the lock-in detection signal of the interference light intensity I_{0F}. When the interference light intensity I_{0F} from equation (14) is synchronized by the lock-in amplifier 1 (LIA1) with the reference signal of 3rd-harmonic sine wave ($\sin 3\omega_m t$), and the lock-in amplifier 2 (LIA2) with the reference signal of 2nd-harmonic cosine wave ($\cos 2\omega_m t$) (see figure 2), two signals of LIA1 and LIA2 can be written as

$$I_{0F}(3\omega_m) = -2E_0E_F J_3(k_{m0})\sin(\varphi'_{int} - \frac{4\pi n}{c}f_0\Delta z) \quad (15),$$

$$I_{0F}(2\omega_m) = 2E_0E_F J_2(k_{m0})\cos(\varphi'_{int} - \frac{4\pi n}{c}f_0\Delta z) \quad (16).$$

The interference light intensity $I_{\pm 2}$ of the $\pm$2nd order diffraction at APD2 is also written as

$$I_{\pm 2} = |E_{+2}|^2 + |E_{-2}|^2$$
$$+2E_{+2}E_{-2}\left[\begin{array}{l}\cos(\varphi'_{\pm 2} - \frac{8\pi}{d}\Delta x)\left\{J_0(k_{m0}) + 2\sum_{m=1}^{\infty}J_{2m}(k_{m0})\cos 2m\omega_m t\right\}\\-\sin(\varphi'_{\pm 2} - \frac{8\pi}{d}\Delta x)\left\{2\sum_{m=1}^{\infty}J_{2m+1}(k_{m0})\cos(2m+1)\omega_m t\right\}\end{array}\right] \quad (17).$$

In the equation (17), $\varphi'_{\pm 2}$ is also an initial phase. When the interference light intensity $I_{\pm 2}$ from equation (17) is

synchronized by the lock-in amplifier 3 (LIA3) with the reference signal of 3rd-harmonic sine wave ($\sin 3\omega_m t$), and the lock-in amplifier 4 (LIA4) with the reference signal of 2nd-harmonic cosine wave ($\cos 2\omega_m t$) (see figure 2), two signals of LIA3 and LIA4 can be written as

$$I_{\pm 2}(3\omega_m) = -2E_0E_F J_3(k_{m\pm 2})\sin(\varphi'_{m\pm 2} - \frac{8\pi}{d}\Delta x) \quad (18),$$

$$I_{\pm 2}(2\omega_m) = -2E_0E_F J_3(k_{m\pm 2})\cos(\varphi'_{m\pm 2} - \frac{8\pi}{d}\Delta x) \quad (19).$$

In the equations (18) and (19), $k_{m\pm 2}$ is also a modulation index. From the equations (15), (16), (18) and (19), we can obtain Lissajous diagram from two reference signals with phase difference of 90degree [16]. Using Lissajous diagram, the axial (Z-axis) and radial (X-axis) displacements of the grating can be calculated concurrently.

3. EXPERIMENTS AND DISCUSSION

We constructed the spindle motion measurement system using three optical sensor as shown in **figure 3**.
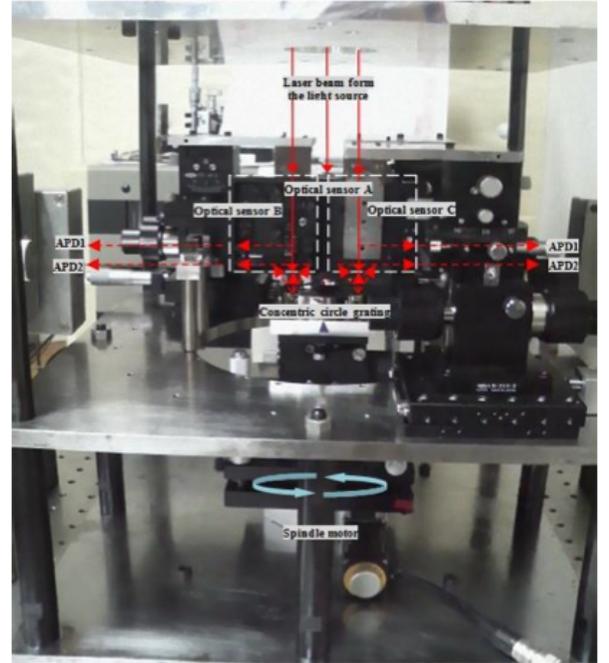

Figure 3 Measurement system for spindle radial, axial and angular motions

An LD (Hitachi, model: HL6344G), with a wavelength of 635 nm and a sinusoidal phase modulation frequency of 33 kHz, was applied to the interferometers as a light source. **Figure 4** shows the photograph of the optical sensor. In the sensor, optics are stiffly fixed in the plate. The optical sensor was fixed over the concentric circle grating. APD1 detected the interference signal of axial (Z-axis) motion and APD2 detected the interference signal of radial (X-axis or Y-axis) motion. The concentric circle grating with the pitch of 2 μm was setup on the spindle motor (Chuo Precision, model: ARS-636-HM). **Figure 5** shows the photograph of

concentric circle grating. The fine concentric circle grating is the key technology for attaining our measurement goal. The grating was fabricated using an ultra-precise numerical control(NC) cutting machine tool (ROBONANO@FANUC) and a sharp single crystal diamond tool with a top radius of less than 1 μm. The material used was stainless steel with nickel phosphide plating of 100 μm thickness. Many grating grooves were formed on the nickel phosphide plate. In the grating, 1000 pitches were formed with a concentric circle structure [13]. We measured spindle radial, axial and angular motions using the system shown in figure 3. **Table 1** lists the specifications of the spindle motor. In the experiment, its maximum speed was 24 degree/sec, or 4 rpm. The measurement conditions applied for the spindle motion are shown in **table 2**.

Figures 6 (a) and (b) show the raw Lissajous diagrams for lateral and vertical displacement from the sensor A shown in figure 3. The Lissajous diagrams are deformed due to variation of the laser intensity. However, lateral and vertical displacements can be determined from these diagrams.
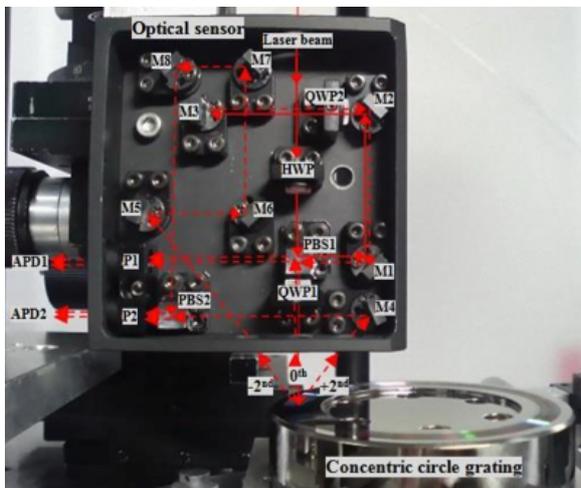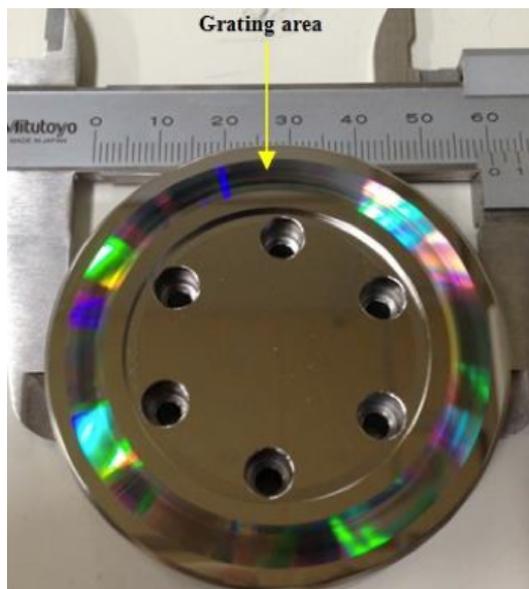

Figure 4 Optical sensor and concentric circle grating

Figure 5 Concentric circle grating

Table 1 Specification of the spindle motor

Diameter of motor stage	60 mm
Accuracy of position	0.15 degree
Axial error (Maximum)	0.06 mm
Radial error (Maximum)	0.03 mm
Maximum speed	24 degree/sec

Table 2 Measurement conditions applied to spindle motion

LD modulation frequency	33kHz
Modulation index	3.67 rad
Modulation bandwidth of LD	1.75 GHz
Revolution speed (Maximum)	40 degree/sec (4 rpm)
Number of rotation	3 rotations
Sampling rate	10 kHz
Cut-off frequency of lock-in amp.	300 Hz
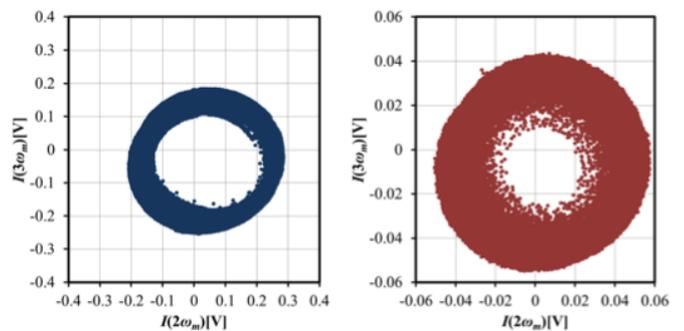
   (a) Z-axis motions   (b) Y-axis motions

Figure 6 Raw Lissajous diagrams for lateral and vertical displacement from the sensor A shown in figures 1 and 3.
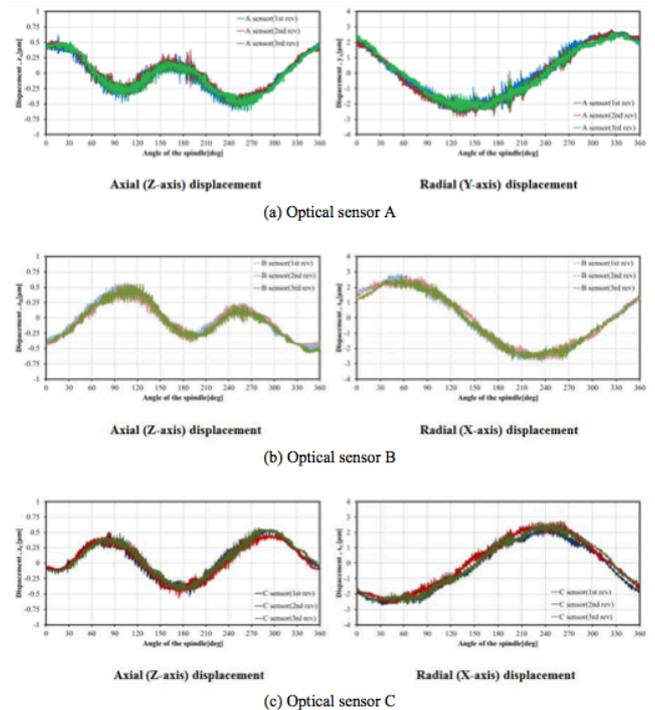

Figure 7 Axial (Z-axis) and radial (X or Y-axis) displacements of the spindle from three optical sensors.

Figure 7 shows the axial (Z-axis) and radial (X or Y-axis) displacement of the spindle motion from three optical sensors A, B and C with 3 rotations. In figure 7, the measurements repeatability of axial (Z-axis) and radial (X or Y-axis) displacements are estimated to be approximately 0.2 μm and 0.3 μm for optical sensor A, 0.4 μm and 0.6 μm for optical sensor B, and 0.4 μm and 0.4 μm for optical sensor C, respectively. The measurement results show that three optical sensors can measure the spindle motions with a good repeatability.

Figures 8 (a), (b) and (c) show the radial, axial and angular motions of the spindle. The centering error also can be seen in figure 8 (a). Using the concentric circle grating three optical sensors, we can measure the spindle radial, axial, and angular motions concurrently.
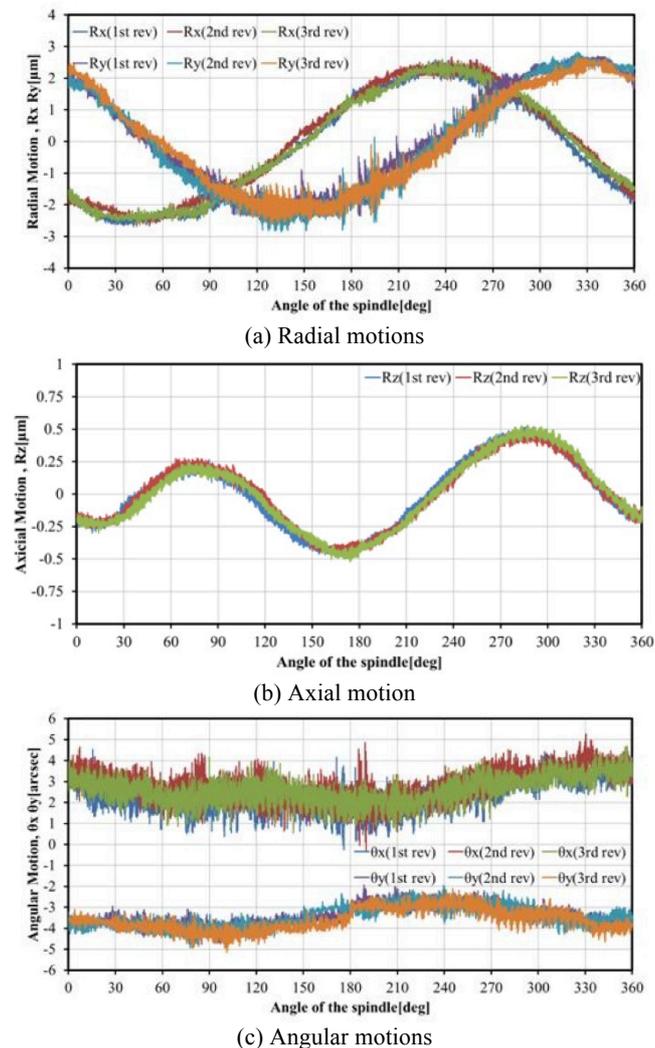

(a) Radial motions

(b) Axial motion

(c) Angular motions

Figure 8 Radial (a), axial (b) and angular (c) motions of spindle.

4. CONCLUSION

In this paper, we have proposed a measurement method using concentric circle grating and phase modulation interferometers to measure the spindle radial, axial, and angular motions concurrently. The measurement principle of the optical sensor using a concentric circle grating to measure the displacement was clarified. The displacement (Lissajous diagram) can be obtained when we add a small modulation to the frequency of the light source. By using three optical sensors, we can measure spindle radial, axial, and angular motions concurrently at the low speed of 4 rpm with the sinusoidal phase modulation frequency of 33 kHz. Based on the results, we are planning to increase the modulation frequency up to several 10 MHz in order to measure the spindle motion at the high speed of 10 krpm, and test the performance of this system in the near future. In the previous paper [16], we clarified that one of the cause of the interpolation error for the two interferometers is polarization mixing. However, to reduce the interpolation error due to amplitude modulation appeared in the laser diode, we need the compensation method in the near future. To remove the air turbulence effect in the measurement system, we will employ a stabilized chamber. To compensate the artifact error of the concentric circle grating, we are also planning to use some error separation methods, such as the reversal method [3].

REFERENCES

[1] R. Grejda, E. Marsh and R. Vallance, Techniques for calibrating spindles with nanometer error motion, Prec. Eng., Vol.29, pp.113-23, 2005.

[2] J. C. Lee, W. Gao, Y. Shimizu, J. Hwang, J. S. Oh and C. H. Park, Spindle error motion measurement of a large precision roll lathe, Int. J. Prec. Eng. Manuf. Vol.13 pp. 861-867, 2012.

[3] R. Donaldson, A simple method for separating spindle error from test ball roundness error, Ann. CIRP, Vol. 21, pp. 125-126, 1972.

[4] E. Marsh, J. Couey and R. Vallance, Roundness measurement of spherical artifacts at arbitrary latitude, Prec. Eng. Vol. 30 pp. 353-356, 2006.

[5] E. Okuyama, N. Nosaka and J. Aoki, Radial motion measurement of high-revolution spindle motor, Measurement, Vol.40, pp. 64-74, 2007.

[6] Y. C. Park and S. W. Kim, Optical measurement of spindle radial motion by Moiré technique of concentric gratings, Int. J. Mach. Tools. Manuf., Vol. 34, pp. 1019-1030, 1994.

[7] A. Kataoka, M. Nomura, O. Horiuchi, T. Shibata and Y. Murakami, A prototype of Radial Encoder, Proc. JSPE Ann. Spring Meeting (Tokyo), pp 513-514, 2008 (in Japanese).

[8] W. Gao, T. Takahara and S. Kiyono, On machine measurement of angular motion of spindle, Proc. ASPE Ann. Meeting (St. Luis), pp. 355, 1998.

[9] I. Ogura and Y. Okazaki, Precision measurement for axial and angular motion errors of turning spindle by using multi point method, J. Japan Soc. Prec. Eng., Vol. 67, pp.1120-1124, 2001.

[10] E. R. Marsh, Precision Spindle Metrology (Pennsylvania: DEStech Publications), 2008.

[11] W. Gao and A. Kimura, A Three-axis displacement sensor with nanometric resolution, Ann. CIRP, Vol. 56 pp.529-532, 2007.

[12] A. Kimura, Y. Arai and W. Gao, A two-degree-of-freedom linear encoder for measurement of position and straightness, Proc. ASPE Ann. Meeting (Portland), pp.550-553, 2008.

[13] M. Madden, M. Aketagawa, Y. Ohkubo, S. Kimura, H. Maruyama, S. Higuchi and E. Okuyama, Proposal of concurrent measurement method for spindle radial, axial and angular motions using concentric circle grating interferometers, Int. J. Surf. Sci. Eng. Vol.3, pp. 242-252, 2009.

[14] O. Sasaki and H. Okasaki, 1986 Sinusoidal phase modulating interferometry for surface profile measurement, Appl. Opt., Vol. 52 pp. 3137-3140, 1986.

[15] A. Dandridge, A. B. Tveten and T. G. Giallorenzi, Homodyne demodulation scheme for fiber optic sensors using phase generated carrier, IEEE J. Quant. Electron., Vol. 18, pp. 1647-1653, 1982.

[16] M. Madden, M. Aketagawa, S. Uesugi, T. Kumagai and E. Okuyama, Spindle error motion measurement using concentric circle grating and phase modulation interferometers, Int. J. Automation Technology, Vol. 7, pp.506-513, 2013.